Dynamic Load–Settlement Performance of Shallow Footings under Varying Vibration Frequencies

Sarab Siham Tawfeeq
Department of Civil Engineering, College of Engineering, University of Tikrit, Salah Al-Din, Iraq
sarab.najem@tu.edu.iq (corresponding author)

Received: 5 August 2025 | Revised: 23 August 2025 | Accepted: 30 August 2025

 DOI: https://doi.org/10.48084/etasr.13867

ABSTRACT

This study investigates the effect of machine-induced vibration on the mechanical behavior of gypsum soils with subsurface cavities, utilizing numerical simulations. The analysis integrates advanced statistical methods, including Principal Component Analysis (PCA) and Multivariate Analysis of Variance (MANOVA), to explore the interactions between critical geotechnical variables, such as settlement, Energy Absorption (*EA*), Initial Stiffness (IS), Inflection Point (IP), secant stiffness at peak and mid-settlement, and ultimate bearing capacity (Q_u). This study modeled subsurface cavities as cylindrical voids, represented the soil degradation by staged reduction of stiffness and strength, and introduced the dynamic loading with specified amplitudes, damping, and frequencies to account for resonance. Wilks' test reported $F = 1.16$, $\lambda = 0.81$, and $p \approx 0.04$, indicating a statistically significant, yet, moderate impact of vibration. The results demonstrate that the vibration increased the settlement by more than 150%, reduced EA by up to 80%, decreased secant stiffness by over 70%, and lowered the ultimate bearing capacity by approximately 60%, particularly in soils with larger cavities and higher dissolution potential. These findings underscore the importance of accounting for dynamic loading in foundation design and point to practical measures, including conservative safety factors, targeted soil improvement, and effective resonance control.

Keywords-gypseous soils; cavities; machine-induced vibration; dynamic loading; settlement response

I. INTRODUCTION

The settlement behavior of shallow foundations subjected to dynamic loads has been a focus of extensive geotechnical research, particularly in contexts involving machine-induced vibrations and cyclic stress conditions. Authors in [1] highlighted the importance of utilizing advanced soil constitutive models in accurately capturing the realistic response of foundations to the repeated loading. Their results revealed that the conventional linear elastic and Mohr-Coulomb models tend to underestimate the settlement, especially at higher vibration amplitudes, compared to models that incorporate small-strain stiffness degradation.

Similarly, authors in [2] examined the role of the foundation geometry and embedment depth under vertical vibration, emphasizing the nonlinear behavior of soil–foundation systems and the significant impact of the excitation force levels. In reinforced systems, authors in [3] demonstrated that the multilayer geocell reinforcement effectively reduced the vibration amplitudes and enhanced damping, with triple-layer systems offering the highest improvement in dynamic performance.

In the context of load–settlement behavior under static or quasi-static loading, authors in [4] combined experimental and numerical methods to evaluate the influence of the relative density in sandy soils. They concluded that higher densities significantly improve the load-bearing behavior. Authors in [5] employed a hybrid ANN-HHO model to accurately predict the settlement of geosynthetic-reinforced abutments, showing a strong correlation with large-scale test data. Authors in [6] further explored the behavior of raft foundations under varying load intensities and foundation sizes using both analytical and 3D finite element models, proposing improved methods for determining the compressed zone thickness and settlement profiles.

Beyond static loading, the traffic-induced and environmental vibrations present additional challenges. Authors in [7] addressed this issue by investigating the post-construction settlement of roadbeds founded on soft clays under traffic-induced vibrations. They introduced a novel vibration reconsolidation approach that captures the settlement mechanisms resulting from repeated dynamic disturbance. In urban tunnelling contexts, authors in [8, 9] simulated train-induced vibrations in saturated clays using coupled FEM and DEM models, respectively. This revealed that higher vibration frequencies lead to increased particle rearrangement and pore pressure buildup, ultimately accelerating the settlement process.

Furthermore, the vibrations transmitted during pile-driving operations were explored in [10], where a measurable settlement effect in the surrounding sandy soils was reported. Both field monitoring and numerical predictions supported the findings. A deeper understanding of the rheological behavior of vibrated soils was provided in [11], where an analytical solution was developed to account for viscoplastic and time-dependent settlement (vibrocreep) in unsaturated sandy soils, emphasizing how the vibration intensity and shear stress affect the long-term deformation. The importance of advanced modeling in predicting the foundation behavior has been hilighted. Authors in [12] demonstrated that nonlinear pile–soil spring models enhance the accuracy of the settlement predictions for piled raft systems under static loading. Similarly, authors in [13] applied extrapolation techniques to incomplete load–settlement curves and found that the predicted ultimate bearing capacity (Q_u) closely aligns with results from the 3D finite element analysis. These findings support the integration of analytical and numerical methods for the reliable evaluation of load–settlement responses. Despite the depth of the existing literature on the vibratory effects, a critical gap remains in understanding the dynamic behavior of shallow foundations resting on collapsible soils, particularly those rich in gypsum, which are prone to strength loss due to dissolution. The current models often neglect the dual influence of the vibration and progressive material degradation on the foundation performance. Moreover, the interaction between the cavity development from gypsum dissolution and cyclic loading has not been sufficiently addressed in numerical simulations.

The objective of this study is to numerically investigate the dynamic response of shallow foundations on gypseous soils with varying degrees of dissolution-induced degradation. Harmonic vertical excitations were simulated using GeoStudio to assess the settlement, stiffness, *EA*, and bearing capacity under different soil types and cavity configurations. Advanced statistical methods were employed to quantify the relative influence of the soil, cavity geometry, and vibration frequency (*HZ*). The aim is to provide practical insights for a safer and more resilient foundation design in collapse-prone gypseous environments.

II. METHODOLOGY

To investigate the dynamic behavior of Soil under machine-induced vibration, a numerical approach was employed using GeoStudio software. The methodology consisted of three core stages: soil characterization, model setup and simulation, and data extraction and interpretation.

A. Soil Classification and Input Parameters

The analysis focused on a square footing subjected to harmonic vertical loads over various types of gypseous soils, representative of a collapse-prone ground commonly found in arid regions [14]. The soils were classified into four types based on their gypsum content and collapse behavior. As presented in Table I, the reference soil was characterized by a high gypsum content and dry strength. In contrast, the other soil types represented various levels of mechanical degradation due to the simulated dissolution. These degradations were modeled indirectly by a staged reduction of stiffness (E) and shear strength parameters (c, φ), following the recommendations in [15], where it was shown that dissolution levels up to 40% can drastically reduce the Bearing Capacity Ratio (BCR) even with favorable *L*/*B* ratios. Parameter reduction was also proposed as a practical proxy in numerical analysis.

The subsurface cavities were explicitly represented as cylindrical voids with circular cross-sections, positioned at depths of 0.5–2.0 m, and horizontal offsets (center, 0.25*B*, 0.5*B*). This geometric form (cylindrical circular cavities) and the adopted *D*/*B* ratios were applied based on the modeling practices of [15, 16], where it was highlighted that the cavity geometry, depth, and horizontal location are decisive factors controlling the reduction in BCR. In particular, authors in [16] showed that BCR decreases by more than 50% when cavities occur at depths close to half the footing width, while authors in [15] demonstrated that dissolution up to 40% severely reduces BCR even with favorable *L*/*B* ratios.

Dynamic loading, in this study, was applied as vertical harmonic sinusoidal excitation to realistically represent the machine-induced vibrations on foundations. Three amplitude levels were defined at 2%, 5%, and 10% of the static footing pressure, thereby covering a practical range from light to heavy operational scenarios. A damping ratio of 5% was incorporated, reflecting commonly accepted values in soil–foundation dynamic interaction and ensuring that the energy dissipation was adequately represented. The waveform of excitation was sinusoidal, with frequencies ranging between 10–30 Hz. This interval was selected both to simulate the operational frequency range of the construction equipment and to approach the natural frequency of the soil–cavity–foundation system. The resonance conditions were examined by comparing the applied excitation frequencies with the computed fundamental frequency of the soil domain, allowing the amplification phenomena to be identified in the simulations. The importance of these parameters—amplitude, damping, waveform, and resonance—has also been emphasized in [17], where it was confirmed that increasing *HZ* reduces IS and enhances the settlement response, thereby reinforcing the adopted modeling strategy in the present analysis.

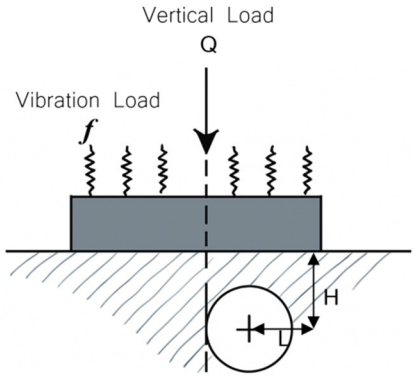

Fig. 1. Schematic of the footing–cavity system under dynamic excitation.

For each soil type, the adopted cavity geometry and degradation strategy reflect both the numerical cavity ratios and soil weakening approaches proposed in [15, 16, 18], ensuring physical relevance and computational efficiency. Figure 1 presents a schematic of the model layout, illustrating the cavity position, excitation input, and key boundary conditions.

The test design, as summarized in Table II, included a comprehensive combination of the soil conditions, vibration frequencies, and cavity positions, resulting in a wide range of simulations. This provided a robust framework for analyzing how the interaction between the gypsum dissolution, vibration, and cavity location influences the foundation stability and deformation.

TABLE I. GEOTECHNICAL PROPERTIES OF REFERENCE GYPSEOUS SOIL AS REPORTED IN [14]

Parameter	Value	Standard/test method
Gypsum content (*GC* %)	0.7388	Calculated
Specific gravity (G_s)	2.380	BS 1377:6B [19]
Liquid limit (*LL* %)	0.260	BS 1377:2A/BS 1377:3 [20, 21]
Plastic limit (*PL* %)	0.210	
Plasticity index (*PI* %)	0.050	
Uniformity coefficient (C_u)	3.00	ASTM D422 [22]
Curvature coefficient (C_c)	0.10	
Gravel/sand/fines (%)	8/74/18	
Soil classification (USCS)	SM-SC	
Initial void ratio (e_0)	0.5163	ASTM D2435-04 / ASTM D5333 - 03 [23]
Compression index (C_c)	0.055	
Recompression index (C_r)	0.011	
Shear strength (dry, c/φ) (ref. soil and soil I)	330 kPa / 49°	ASTM D3080/D3080M[24]
Shear strength (after soaking 6h) (soil II)	28 Kpa / 43°	
Shear strength (after soaking for 24h) (soil III)	19 kPa / 44.5°	

TABLE II. EXPERIMENTAL MATRIX AND MODEL DISTRIBUTION

Soil type	Vibration frequencies (Hz)	Vertical cavity depths (*H*, cm)	Horizontal offsets (*L*, cm)	Models simulated
Ref. Soil	0,10, 20, 30	None	None	4
Soil I	10, 20, 30	0.5, 1, 2	Center, 0.25, 0.5	27
Soil II	10, 20, 30	0.5, 1, 2	Center, 0.25, 0.5	27
Soil III	10, 20, 30	0.5, 1,2	Center, 0.25, 0.5	27
Total				85

B. Numerical Modeling in Geostudio

The simulation domain was designed with sufficient width and depth to minimize the boundary effects. A refined mesh was applied near the loading area and cavity zones using triangular finite elements to capture the stress gradients with high precision [15, 25]. The boundary conditions included fixed supports at the base and horizontal fixity at the lateral boundaries, while the top surface remained free to deform vertically. Vertical static loading was applied incrementally to simulate the footing pressure, and dynamic loads were superimposed where required. The focus was on generating load–settlement curves under various conditions of soil type, *HZ*, and cavity location.

1) Limitations

Although the developed model effectively simulates the soil–foundation response under vibrational loading, the gypsum dissolution was represented indirectly through parameter reduction. A fully coupled hydro-mechanical model could capture the progressive dissolution and cavity evolution with greater accuracy, but it requires extensive calibration data and higher computation demand.

C. Curve Extraction and Mechanical Parameter Evaluation

From each load–settlement curve, several critical mechanical parameters were extracted to evaluate the soil response under combined static and dynamic loading. These parameters were chosen to reflect both the strength and deformation characteristics of the Soil, serving as indicators of the performance degradation due to the presence of cavities and vibration effects. Table III summarizes the extracted variables, their calculation methods, and their physical significance in the context of geotechnics.

TABLE III. VARIABLES DERIVED FROM LOAD–SETTLEMENT CURVE

Variable name	Symbol, Unit	Calculation method	Engineering significance
Ultimate bearing capacity	*Qu*, kPa	Max vertical stress before failure	Indicates soil strength and load-carrying capacity
Settlement	*S*, mm	Vertical axis value at Q_u	Reflects deformability under load
Initial stiffness	*IS*, kN/mm	Slope of load–settlement curve at origin ($\Delta Q/\Delta S$)	Indicates soil rigidity before plastic deformation
Secant stiffness at Q_u	K_{max}, kN/mm	Q_u/S	Measures average stiffness across the entire loading phase
Secant stiffness at $Q_{u50\%}$	$K_{50\%}$, kN/mm	$Q_{u50\%}/ S_{50\%}$ (settlement at 50% Q_u)	Provides insight into the elastic behavior in the early phase
Inflection point	*IP*, mm	Inflection or turning point of the curve (from the 2nd derivative)	Marks the transition from the elastic to the plastic response
EA	*EA*, kN·mm	Area under load–settlement curves up to Q_u	Indicates the soil's ability to absorb energy before failure

These metrics were essential for comparing the behavior of different soil types and evaluating the sensitivity of each mechanical property to the vibration effects and internal weakening (cavities/dissolution). Their inclusion provides a deeper quantitative understanding of how the vibration alters the performance envelope of gypsum soils.

III. RESULTS

A. Model Validation under Vibration Frequency (HZ)

To ensure the accuracy and reliability of the developed numerical model, a validation was conducted by comparing it

with experimental data under a dynamic excitation of 30 Hz, as reported in [17]. Both the numerical and experimental results were normalized to facilitate an objective comparison of the displacement behavior. As illustrated in Figure 2, the numerical response closely tracks the experimental curve across the entire loading range, with a firm fit in the nonlinear domain. This consistency highlights the model's ability to simulate the stress–strain response of gypseous soils under vibratory loading conditions. The statistical evaluation of the match yielded a coefficient of determination ($R^2 = 0.984$), indicating a very high degree of linear correlation. Additionally, the Root Mean Square Error (RMSE) and Mean Absolute Error (MAE) were 0.027 and 0.022, respectively, reflecting a minimal deviation and high predictive accuracy.

These results confirm that the numerical model not only captures the general trend of the soil behavior under vibrational loading, but also provides a reliable quantitative prediction of the load–settlement response. The successful validation reinforces the credibility of the subsequent simulations and enhances the confidence in the conclusions derived throughout this study.

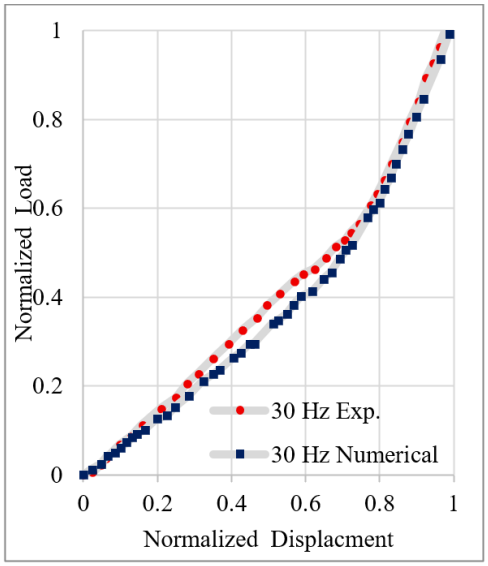

Fig. 2. Model validation under *HZ*.

B. Statistical Analysis for the Load Settlement Curve Output

The statistical analysis enhanced the scientific validity of the study by confirming that the observed soil responses were systematic and reproducible rather than numerical artefacts. This strengthened the reliability of the numerical model and provided confidence in the generalization of the findings [26]. Figure 3 (boxplot) presents a detailed analysis of the statistical distribution of data related to soil performance under the influence of vibrations, highlighting the key variables. The data show an asymmetric distribution in some variables, particularly in *EA*, where the media is skewed away from the center between the first and third quartiles. This indicates a slight deviation from a normal distribution but remains within a reasonable range. Outliers are evident in the boxplot, which represent soils lacking cavitation, gypsum dissolution, or vibrations, explaining the presence of these exceptional values as they were used as comparison samples in the study. While these outliers may appear atypical, they offer valuable insights into the variation between the soils, regarding the effects of the vibrations and cavitation on their mechanical properties.

On the other hand, variables, such as IS and settlement, show moderate variability within the interquartile range, reflecting stability in the soil performance when subjected to load and vibration testing. This further supports the reliability of the data and confirms the stability of certain mechanical factors.

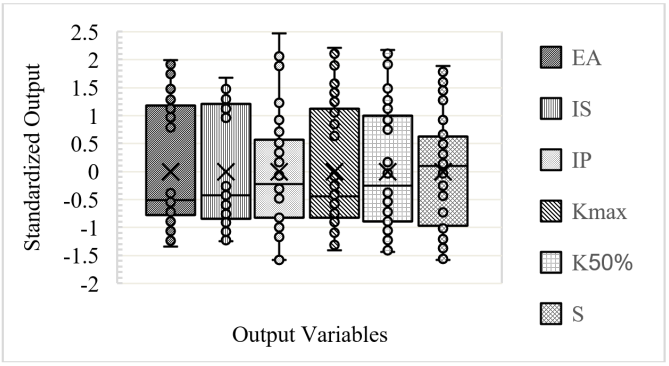

Fig. 3. Boxplot visualization of key mechanical parameters across soil types under vibration effects.

Figure 4 presents the results of the Grubbs Test for several mechanical properties measured by load-settlement curves. Upon examining the chart, it is evident that the observed values (*G* Observed) for all variables remain below the critical values (*G* Critical), suggesting that the data conform to acceptable statistical limits. The *p-value* for all the variables indicates the absence of any outliers, as it was one across all measured parameters, further reinforcing the reliability and consistency of the data. This outcome aligns with the findings from Figure 3, which indicates the stability of the soil's mechanical performance without any exceptions or deviations in both analyses. The consistency between the Grubbs Test and the Boxplot results underscores the overall balance in the data, confirming the accuracy of the analysis and ensuring the data readiness for further in-depth analysis in subsequent stages.

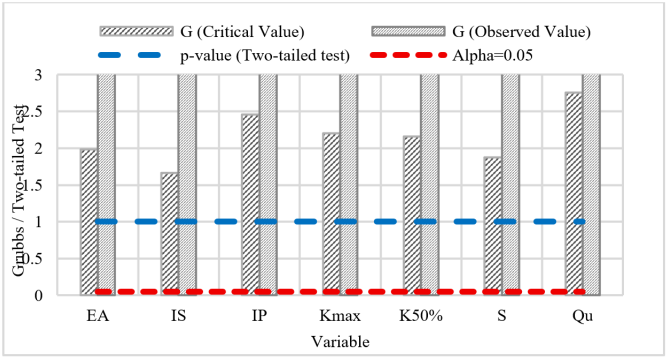

Fig. 4. Statistical outlier identification via two-tailed Grubbs' test for load–settlement parameters.

PCA was performed to reduce the dataset's dimensionality and identify the most influential variables affecting the geotechnical response of soils under loading [27, 28]. The analysis included a comprehensive set of mechanical parameters measured by load-settlement curves. As illustrated in Figure 5 (Scree plot), the first two principal components (*F1* and *F2*) together explain 88.25% of the total variance (*F1* = 61.50%, *F2* = 26.75%), indicating a highly compact representation of the dataset.

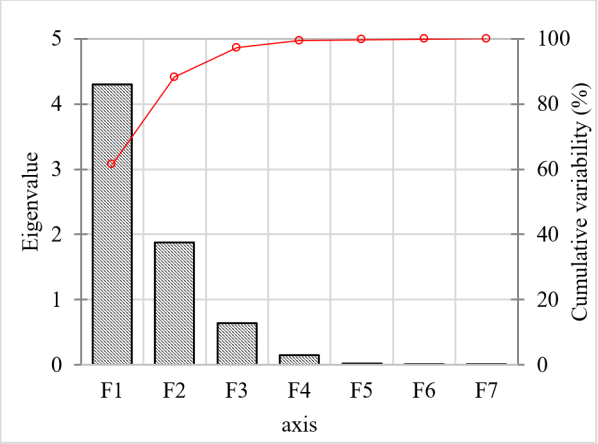

Fig. 5. Eigenvalue distribution across principal components (Scree plot).

The factor loadings reveal that *F1* is strongly influenced by *K50%* (0.985), *Kmax* (0.965), *EA* (0.957), and *IS* (0.835), making it interpretable as a composite mechanical stiffness index. Meanwhile, *F2* is primarily driven by *IP* (0.809) and S (0.733), suggesting its representation of the ductility and failure deformation behavior. The variable *Qu* displays a divergent direction in the Biplot, as seen in Figure 6, indicating a less correlated or nonlinear behavior, relative to the *F1*-associated mechanical indices. This divergence may be attributed to the inclusion of various soil types in the dataset, some of which lack dissolution properties, internal cavities, or exposure to vibration. These samples were introduced deliberately for comparative purposes, which may have led to outlier behavior in the PCA results. Therefore, while the first component (*F1*) offers a robust foundation for evaluating the overall mechanical response of soils, Q_u should be treated as a distinct resistance parameter, whose behavior is influenced by the soil type and may require dedicated analysis in future investigations.

The biplot in Figure 6 reveals distinct behavioral trends among the tested soil conditions. The points concentrated in the upper-right quadrant are associated with higher deformation-related indicators, reflecting soils with greater susceptibility to displacement and energy dissipation under dynamic excitation. This region corresponds to cases where the soil structure has been weakened—either by dissolution processes or the presence of geometrically unfavorable cavities—leading to reduced stiffness and increased settlement. In contrast, the points located in the lower-left quadrant exhibit stronger resistance to vibration-induced deformation. These samples appear to retain higher secant stiffness and lower *EA*, indicating soils with a stable internal structure, minimal degradation, and no significant cavity effects. The distribution of data along the principal components highlights the combined influence of the mechanical degradation, cavity configuration, and excitation frequency. It suggests that a single parameter does not govern the soil response, but rather the complex interaction of the material properties and loading geometry. Such a dimensional reduction is proved to be valuable in identifying patterns of anomalous behavior and separating the stable from the failure-prone soil profiles.

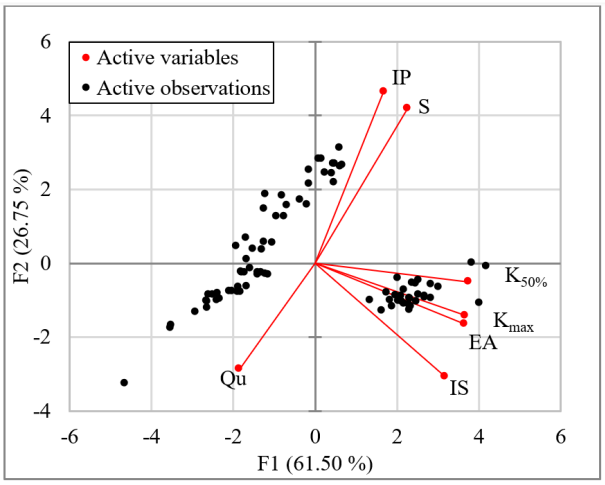

Fig. 6. Multivariate distribution of soil behavior based on PCA biplot.

To complement the PCA findings, MANOVA was conducted to evaluate the significance of four key factors: soil type, cavity depth (*H*), cavity horizontal location (*L*), and *HZ*. As illustrated in Figure 7, the tests (Wilks' Lambda, Hotelling's Trace, Pillai's Trace, and Roy's Root) confirm the dominant influence of the soil type (Wilks' $\lambda = 0.00$, $F = 3.04$) and cavity depth ($\lambda = 0.21$, $F = 5.21$), with the horizontal distance *L* also showing a notable impact ($\lambda = 0.30$–0.25, $F = 1.58$–2.46). Although *HZ* exhibited the least statistical significance across the four tests (e.g., Wilks' $\lambda = 0.81$, $F = 1.16$), its values remain within acceptable influence ranges, indicating that it does affect mechanical responses, such as *EA* and settlement, albeit to a lesser extent. The consistency of moderate λ values (0.21–0.30) across methods supports its inclusion in the analysis, particularly due to its relevance to the practical excitation conditions.

In summary, all tested factors contributed to the variation in the soil response, with vibrational frequency (*HZ*) showing the weakest but still a measurable effect, reinforcing its consideration in dynamic design scenarios.

C. Soil Response under Load and Cavity Influence

Figure 8 demonstrates the varying influence of different soil types on the load–settlement relationship. The reference soil and Soil I exhibit more cohesive and stable behavior under loading conditions. This can be attributed to the relatively intact gypsum structure in these soils, which lacks significant dissolution features or internal voids. As a result, they maintained relatively low settlement values even under increasing loads. In contrast, Soil II and Soil III display weaker

and more ductile responses. These behaviors are primarily linked to higher levels of gypsum solubility and increased internal cavity sizes, which reduce the soil's load-bearing capacity. The degradation of the gypsum matrix under stress leads to the weakening of the bond and collapse of the internal structure, resulting in accelerated settlement with minimal load increments.

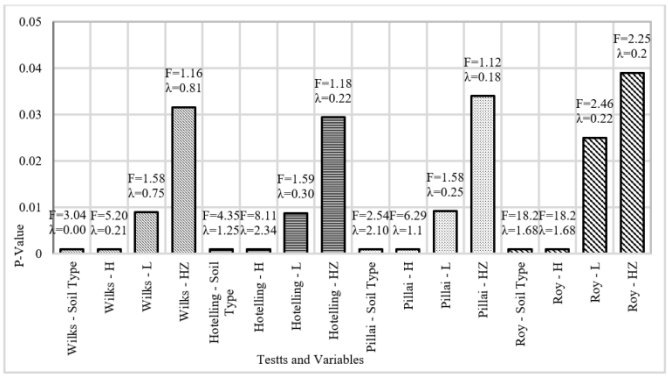

Fig. 7. Statistical significance of *HZ* and Soil type via MANOVA.

Figure 9 portrays the influence of the cavity position, relative to the loading point, on the geotechnical performance. The presence of a cavity directly beneath the center of the footing (at $H/L = 1$) results in a critical response, characterized by a brittle behavior and rapid failure. This is due to the soil mass above the cavity's inability to redistribute stress effectively. In contrast, the cavities located farther from the load axis (e.g., $H/L = 2$ and 4) allow the surrounding soil to provide lateral support and a more gradual load redistribution, enhancing the stability and reducing the deformation rates. These observations underscore the high sensitivity of gypsum soils to the spatial configuration of subsurface voids; even when the soil type remains constant, performance varies drastically with the changes in the cavity location.

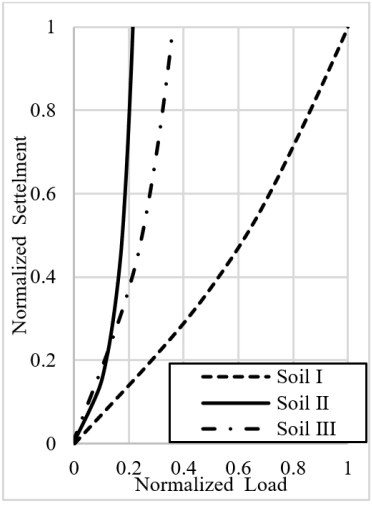

Fig. 8. Normalized load–settlement curves for different soil types under dynamic loading.

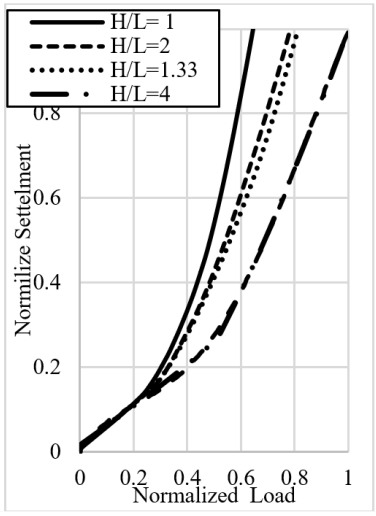

Fig. 9. Normalized load–settlement curves for varying horizontal cavity offsets (L) at constant depth (H).

D. Normalized Load–Settlement Curve Response to Vibrational Frequency

Figure 10 displays the effect of the vibration on the load–settlement response of the reference soil samples without cavities. Under normalized loading, the static case exhibits a smoother and more gradual increase in settlement. In contrast, the vibration scenario indicates a slightly higher resistance to settlement at initial loads but demonstrates accelerated deformation at higher loads. This trend is consistent with the general mechanical behavior of soils under cyclic or dynamic loading, where stiffness degradation occurs due to particle rearrangement and microstructural changes. The samples were tested under vibration with subsurface cavities, all of which exhibit amplified settlement responses relative to the reference curves. This highlights the detrimental interaction between the vibration and cavity presence, particularly in gypsum soils where the dissolution and internal weaknesses intensify the deformation mechanisms.

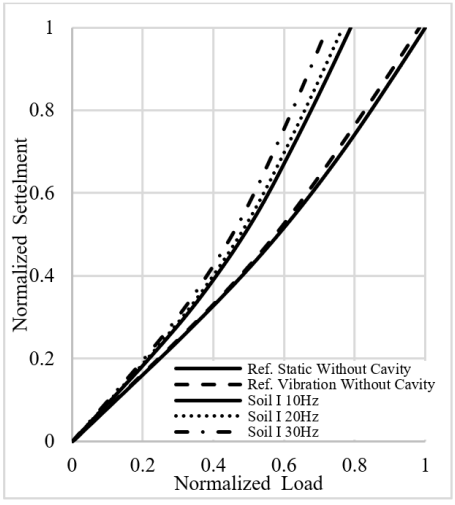

Fig. 10. Normalized load–settlement response for Soil I under different *HZ* compared to reference conditions.

E. Energy Absorption versus Cavity Distance for Various Frequencies

Figure 11 illustrates the impact of the horizontal cavity position (*L*) on *EA* at various vibration frequencies, with a fixed cavity depth (*H* = 1 m). Across all frequencies, *EA* follows a U-shaped trend, with the lowest value occurring when the cavity is positioned at mid-distance (L ≈ 0.25 m). This suggests a critical interaction zone, where the stress distribution is disrupted the most, minimizing the soil's capacity to dissipate energy. As the cavity moves closer to the center or toward the boundary, *EA* increases, indicating more stable redistribution paths for stress transfer. Additionally, frequency plays a clear role: higher frequencies (e.g., 30 Hz) result in lower overall *EA*, which aligns with the expected increase in the soil stiffness degradation and dynamic instability under more intense vibratory loading. The consistent trend across frequencies further confirms the sensitivity of the gypsum soil to both the vibrational intensity and cavity location.

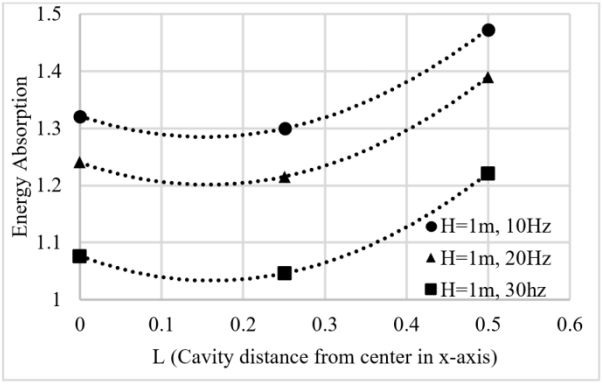

Fig. 11. Effect of cavity horizontal offset (*L*) on *EA* at various *HZ*.

F. Engineering Implications for Design and Mitigation

The numerical and statistical results carry an engineering significance. The strong influence of the soil type confirms that the foundations placed on highly dissolvable gypsum (Soils II and III) require either prior stabilization (e.g., cement grouting or chemical treatment) or adoption of deep foundation systems to bypass the weak zones. The critical impact of the cavity position, particularly that of cavities directly beneath the footing center, highlights the need to either increase the footing depth or avoid the construction in cavity-prone alignments. The amplified settlements observed under vibrational loading emphasize that the resonance effects must be considered in practice, suggesting operational adjustments to the machinery frequencies or the inclusion of structural damping systems.

The U-shaped *EA* response further identifies the intermediate cavity offsets (*L* ≈ 0.25B) as particularly critical zones, where targeted soil improvement or load redistribution measures should be applied. Finally, given the consistent reduction in stiffness and capacity across multiple scenarios, the safety factors in design should be conservatively increased for the foundations in gypsum-rich soils. These implications provide a pathway for translating the numerical findings into practical geotechnical strategies that enhance the foundation resilience against the cavity formation and vibrational loads.

IV. CONCLUSIONS

This study employed numerical simulations using the GeoStudio software to investigate the mechanical behavior of different soil types under vibrational loading conditions, considering various cavity locations and frequencies. The multivariate statistical approach, coupled with direct numerical outputs, offered an understanding of the interactive effects among the soil characteristics, cavity configurations, and excitation frequencies. The key findings of this study are:

- Soil composition emerged as the most influential factor affecting the deformation behavior. Compared to the reference soil, highly dissolvable soils exhibited a marked reduction in the energy absorption (*EA*) capacity (by more than half) and a notable increase in the vertical settlement, indicating a substantial decline in the mechanical resistance under load.
- The cavity geometry and location significantly altered the load–settlement response. Cavities located at intermediate distances from the load center produced the most pronounced deformations, resulting in noticeably higher settlements. In contrast, deeper or more distant cavities led to relatively moderate impacts, highlighting the critical role of the spatial configuration.
- Although the effect of vibration frequency (*HZ*) was statistically less dominant, consistent indicators across Multivariate Analysis of Variance (MANOVA) tests suggest that even moderate-frequency excitation contributes to measurable changes in the stiffness and settlement, underscoring its relevance in the vibrational analysis of geotechnical systems.
- The results from Principal Component Analysis (PCA) and biplot analyses confirmed a strong correlation between the energy-related indicators (e.g., Secant stiffness and absorption) and principal components, helping to isolate the key variables responsible for the soil instability under cyclic loading.
- The combined graphical analysis (e.g., boxplots, biplots) and MANOVA statistics effectively demonstrated that both the mechanical and geometric parameters act synergistically, influencing the overall bearing capacity and stability of soils with subsurface cavities.

These findings contribute to a deeper understanding of the soil-structure interaction under vibratory loads, offering guidance for the design and evaluation of foundations in regions prone to subsurface voids or subjected to dynamic machinery.

Future research should focus on incorporating hydro-mechanical coupling to simulate the progressive gypsum dissolution more accurately and on validating the numerical results through controlled field-scale vibration tests.

REFERENCES

[1] S. Alzabeebee and S. Keawsawasvong, "Dynamic Response of a Machine Foundation Using Different Soil Constitutive Models," *Transportation Infrastructure Geotechnology*, vol. 11, no. 1, pp. 426–445, Feb. 2024, https://doi.org/10.1007/s40515-023-00284-4.

[2] K. Tandon, R. Ralli, B. Manna, and G. V. Ramana, "Vertical Vibration Tests to Study the Effect of Foundation Geometry and Embedment on the Non-linear Response of Block Foundations," *Arabian Journal of Geosciences*, vol. 16, no. 12, Dec. 2023, Art. no. 663, https://doi.org/10.1007/s12517-023-11773-8.

[3] A. Amiri, S. N. Moghaddas Tafreshi, and A. R. Dawson, "Vibration Response of Machine Foundations Protected by Use of Adjacent Multi-layer Geocells," *Geotextiles and Geomembranes*, vol. 51, no. 4, pp. 15–35, Aug. 2023, https://doi.org/10.1016/j.geotexmem.2023.03.001.

[4] B. Ateş and E. Şadoğlu, "Experimental and Numerical Investigation of Load-Settlement Behaviour to Model Shallow Foundation rest on Sandy Soil," *Erzincan Üniversitesi Fen Bilimleri Enstitüsü Dergisi*, vol. 14, no. 2, pp. 686–703, Aug. 2021, https://doi.org/10.18185/erzifbed.862650.

[5] M. N. Amjad Raja, S. T. Abbas Jaffar, A. Bardhan, and S. K. Shukla, "Predicting and Validating the Load-settlement Behavior of Large-scale Geosynthetic-reinforced Soil Abutments Using Hybrid Intelligent Modeling," *Journal of Rock Mechanics and Geotechnical Engineering*, vol. 15, no. 3, pp. 773–788, Mar. 2023, https://doi.org/10.1016/j.jrmge.2022.04.012.

[6] V. Le Ba, N. Nguyen Van, and K. Le Ba, "Study on the Settlement of Raft Foundations by Different Methods," *MATEC Web of Conferences*, vol. 251, 2018, Art. no. 04054, https://doi.org/10.1051/matecconf/201825104054.

[7] F. Xia, T. Xia, and Z. Wang, "Dynamic Response and Settlement Cause Analysis of Roadbed–Soft Clay Foundation System Under Traffic Vibration Loads," *Applied Sciences*, vol. 15, no. 4, Feb. 2025, Art. no. 2163, https://doi.org/10.3390/app15042163.

[8] Q. Huang, H. Huang, B. Ye, D. Zhang, L. Gu, and F. Zhang, "Dynamic Response and Long-term Settlement of a Metro Tunnel in Saturated Clay Due to Moving Train Load," *Soils and Foundations*, vol. 57, no. 6, pp. 1059–1075, Dec. 2017, https://doi.org/10.1016/j.sandf.2017.08.031.

[9] J. Wang *et al.*, "Numerical Simulation of Land Subsidence Caused by Subway Train Vibration Using PFC," *Proceedings of the International Association of Hydrological Sciences*, vol. 382, pp. 559–564, Apr. 2020, https://doi.org/10.5194/piahs-382-559-2020.

[10] G. Abate, M. R. Massimino, and M. Maugeri, "Settlements Of Sand Caused By Vertical Vibrations: Experimental Versus Numerical Results," in *the 5th International Conference on Earthquake Geotechnical Engineering*, Santiago, Chile, Jan. 2011, vol. 10, Art. no. 13.

[11] A. Z. Ter-Martirosyan, A. N. Shebunyaev, and E. S. Sobolev, "Settlement of a Foundation on an Unsaturated Sandy Base Taking Vibrocreep into Account," *Axioms*, vol. 12, no. 6, Jun. 2023, Art. no. 594, https://doi.org/10.3390/axioms12060594.

[12] S. Karmakar, R. Ranjan, and V. S. Phanikanth, "Response of Pile and Piled Raft Under Static Loads—A Review of Pile Soil Spring Formulations Along with a Case Study," in *Proceedings of the 3rd International Conference on Advances in Concrete, Structural, and Geotechnical Engineering—Volume 3*, vol. 31, S. B. Singh, M. Gopalarathnam, and N. Roy, Eds., Singapore: Springer Nature Singapore, 2025, pp. 191–207.

[13] H. T. Tra, Q. T. Huynh, and S. Keawsawasvong, "Estimating the Ultimate Load Bearing Capacity Implementing Extrapolation Method of Load-Settlement Relationship and 3D-Finite Element Analysis," *Transportation Infrastructure Geotechnology*, vol. 11, no. 4, pp. 2764–2789, Aug. 2024, https://doi.org/10.1007/s40515-023-00332-z.

[14] T. Schanz and H. H. Karim, "Geotechnical Characteristics of Some Iraqi Gypseous Soils," *MATEC Web of Conferences*, vol. 162, 2018, Art. no. 01005, https://doi.org/10.1051/matecconf/201816201005.

[15] S. S. Tawfeeq, "An Analysis of the Bearing Capacity Ratio of the Cavitation-Prone Gypsum Soil," *Engineering, Technology & Applied Science Research*, vol. 15, no. 4, pp. 25235–25243, Aug. 2025, https://doi.org/10.48084/etasr.12010.

[16] A. Al-Obaidi and R. S. Najim, "Estimation of Bearing Capacity Dropping Due to Cavities from Gypseous Soils Melting," *Key Engineering Materials*, vol. 857, pp. 409–416, Aug. 2020, https://doi.org/10.4028/www.scientific.net/KEM.857.409.

[17] N. Alsanabani and A. Alnuaim, "Influence of Vertical Vibration on the Bearing Capacity of Foundation Resting on Salt-encrusted Flat Soil Improved by Cement," *Journal of King Saud University - Engineering Sciences*, vol. 36, no. 2, pp. 122–127, Feb. 2024, https://doi.org/10.1016/j.jksues.2022.11.003.

[18] A. Benbouza, T. Mansouri, and K. Abbeche, "Behavior of Strip Footing/s above Void in Sandy Soil," *Engineering, Technology & Applied Science Research*, vol. 13, no. 1, pp. 10039–10044, Feb. 2023, https://doi.org/10.48084/etasr.5494.

[19] *Methods of Test for Soils for Civil Engineering Purposes: Part 3 Chemical and Electro-chemical Tests*, BS 1377-3, British Standards Institute, London, UK, 1990.

[20] *Methods of Test for Soils for Civil Engineering Purposes: Part 2: Classification Tests*, BS 1377-2, British Standards Institute, London, UK, 1990.

[21] *Methods of Test for Soils for Civil Engineering Purposes: Part 1: General Requirements and Sample Preparation*, BS 1377-1, British Standards Institute, London, UK, 1990.

[22] *Standard Test Method for Particle-Size Analysis of Soils*, ASTM D422-63, ASTM International, West Conshohocken, PA, USA, 2007.

[23] *Standard Test Methods for One-Dimensional Consolidation Properties of Soils Using Incremental Loading*, ASTM D2435/D2435M-11, ASTM International, West Conshohocken, PA, USA, 2011.

[24] *Standard Test Method for Direct Shear Test of Soils Under Consolidated Drained Conditions*, ASTM D3080-04, ASTM International, West Conshohocken, PA, USA, 2004.

[25] A. A. J. Jamel and H. F. Hassan, "Effect of Core Angle in Earth Dam on Seepage Characteristic (Numerical Model)," *Tikrit Journal of Engineering Sciences*, vol. 32, no. 1, pp. 1–10, Mar. 2025, https://doi.org/10.25130/tjes.32.1.26.

[26] R. A. Hussain and A. Al-samarrae, "Theoretical Analysis and Development of an Artificial Neural Network Model to Evaluate Earthen Dam Slope Stability: Theoretical Analysis," *Tikrit Journal of Engineering Sciences*, vol. 29, no. 4, pp. 1–9, Nov. 2022, https://doi.org/10.25130/tjes.29.4.1.

[27] A. A. Jamel, R. A. Hussain, and S. S. Tawfeeq, "Improving Energy Dissipation on Stepped Spillways (Numerical Simulation)," *International Review of Civil Engineering*, vol. 16, no. 3, 2025.

[28] M. I. Ali, A. A. J. Jamel, and S. I. Ali, "The Hardened Characteristics of Self-compacting Mortar Including Carbon Fibers and Estimation Results by Artificial Neural Networks," in *2nd International Conference on Materials Engineering and Science*, Baghdad, Iraq, 2020, vol. 2213, Art. no. 020159, https://doi.org/10.1063/5.0000177.